Mechanical stability of substrate-bound graphene in contact with aqueous solutions

Published in:
2D Materials

Document Version:
Publisher's PDF, also known as Version of record

Queen's University Belfast - Research Portal:
Link to publication record in Queen's University Belfast Research Portal

2D Materials

CrossMark

Mechanical stability of substrate-bound graphene in contact with aqueous solutions

Matěj Velický[1], **Adam J Cooper**[2], **Peter S Toth**[1], **Hollie V Patten**[1], **Colin R Woods**[3], **Konstantin S Novoselov**[3] **and Robert A W Dryfe**[1]

[1]   School of Chemistry, University of Manchester, Oxford Road, Manchester M13 9PL, UK
[2]   School of Materials, University of Manchester, Oxford Road, Manchester M13 9PL, UK
[3]   School of Physics and Astronomy, University of Manchester, Oxford Road, Manchester M13 9PL, UK

E-mail: matej.velicky@manchester.ac.uk and robert.dryfe@manchester.ac.uk

Keywords: graphene, strain, mechanical stability, liquid deposition, Raman spectroscopy

Abstract

We report on the damage caused to mechanically exfoliated monolayer graphene, bound to silicon dioxide substrate, upon contact with liquids. This phenomenon is of significant importance for a wide range of applications where monolayer graphene sheets are used with liquids, especially as an electrode material in electrochemical applications such as energy storage and conversion. Liquid-induced damage to SiO_2-bound graphene was previously observed with a range of solvents. A recently developed microdroplet system, used for a detailed examination of this behaviour, reveals that few-layer graphene flakes down to a bi-layer are stable with respect to aqueous electrolyte droplet formation, but the stability of these droplets is significantly reduced on monolayer graphene and irreversible rupture of the underlying graphene flake occurs. This damage, which we attribute to the presence of nanoscale defects and high adhesion between the graphene and the substrate, seems specific to plasma-cleaned SiO_2 substrates and is not observed on flakes transferred to other substrates. Furthermore, the introduction of impurities, in the form of both polymer residues and native impurities between the flake and the SiO_2 substrate, significantly enhance graphene's immunity to external strain as shown by optical microscopy, atomic force microscopy, and Raman spectroscopy.

Introduction

Average lateral diameters of mechanically exfoliated (ME) graphene flakes have increased significantly since the discovery of graphene, from tens of microns to millimetre dimensions [1]. In terms of structural purity and crystallinity, ME is strongly considered to produce the most appropriate form of graphene for the employment in fundamental studies. This method of preparation requires considerable skill and experience, which could be the main reason why very few research groups reported on electrochemistry of ME graphene flakes [2–5]. As a consequence, chemical vapour deposition (CVD) graphene, as well as few-layer graphene sheets prepared via liquid-phase exfoliation or reduction of graphene oxide, are often substituted for ME graphene for simplicity and scalability [6–9]. However, these alternatives often yield graphene prepared in an uncontrolled and ill-defined manner, which is reflected by inconsistencies between the conclusions drawn about the electrochemistry of graphene [2, 3, 7, 8, 10, 11].

Valota *et al* first noticed significant liquid-induced damage on monolayer ME graphene during attempts to measure the electrochemical response of such samples [3]. The sub-millimetre size flakes broke up when an excess liquid was placed over the graphene. Suspecting that the liquid-induced damage initiates at the graphene edge, a system, utilizing a droplet of electrolyte solution deposited on the basal plane of graphene flake, was introduced [12]. This prevented contact between the liquid and flake edges and had the advantage of a well-defined contact area. The main challenge associated with this setup lies in determining the optimum combination of solvent and electrolyte; it is necessary that the liquid droplets do not evaporate over sufficiently long timescales and are of appropriate hydrophobicity/hydrophilicity, such that complete spreading or de-wetting of the graphene surface is avoided. It was found that 6 M LiCl aqueous solution

was suitable for this purpose. Nevertheless, Toth *et al* [4], and recently Velický *et al* [5] have reported persistent damage upon droplet deposition on the basal plane of graphene, ruling out the presence of edges as the sole cause for the flake breakage. It was found that monolayer graphene is subject to damage upon contact with various solvents, including ethylene glycol, glycerol and silicone oil [4]. Other authors also reported water-induced damage in epitaxial graphene [13].

Contamination of graphitic surfaces with adventitious hydrocarbons or polymer residues from lithographic processing is a known issue [5, 14, 15]. It has previously been shown that fresh surface of supported graphene is actually more hydrophilic than initially thought, whereby graphene's hydrophobicity is a measure of airborne hydrocarbon contamination [16]. Thus, water exhibits strong wetting on freshly cleaved graphite/graphene surface and the contact angle between the two is significantly smaller than that on atmospherically aged samples. The ageing process of graphene occurs within minutes, and therefore any measurements performed on graphene's basal plane, from contact angle measurement to electrochemical scan or charge carrier mobility measurement, should take into consideration the 'freshness' of the graphene surface. Furthermore, it has been suggested that monolayer graphene is actually transparent to wetting [16–18], and therefore is heavily influenced by the underlying substrate.

It is imperative that the liquid-induced instability and the resulting breakage of graphene, which have detrimental effects on the electrochemical performance of graphene-based electrodes, as well as its viability as a protective coating in corrosion protection studies [19–21], are understood and prevented. Herein, we clarify the nature of the liquid-induced damage to SiO_2-bound graphene and find flake preparation procedure allowing stable liquid deposition, in order to aid further research, which requires use of substrate-bound graphene in contact with liquids.

Methods

Chemicals
Acetone ($\geqslant$99.0%), ethanol ($\geqslant$99.0%), and lithium chloride (99%), were purchased from Sigma-Aldrich, UK. Methyl isobutyl ketone (MIBK, 99.0+%), isopropyl alcohol (IPA, 99.5%) and potassium hydroxide (>99%) were obtained from Fisher Scientific UK. Poly (methyl methacrylate) (PMMA, 3% in anisole) was purchased from MicroChem Corp, MA, USA. All chemicals were used as received. LiCl aqueous solutions were prepared using deionized (DI) water of 18.2 MΩ cm resistivity purified via a Milli-Q Direct 8 unit (Merck Millipore, USA).

Flake preparation
All graphene samples were prepared by mechanical exfoliation of graphite onto insulating SiO_2 substrates (either 90 nm or 290 nm thick layer of SiO_2 on Si, IBD Technologies, UK). Prior to flake transfer, SiO_2 wafers were de-greased via sonication in acetone and IPA, 10 min in each solvent, using a TI-H-5 ultra-sonic bath (Elma Hans Schmidbauer GmbH, Germany), dried using compressed nitrogen gas and finally cleaned (10 min), using a low-power oxygen plasma etcher (MiniLab 125, Moorfield, UK), to remove any surface contamination. Natural graphite crystals (NGS, Naturgraphit, GmbH, Germany) were cleaved using a BT-150E-KL cello-tape (TELTEC GmbH, Germany) and pressed onto the SiO_2 wafer. The tape was then dissolved in MIBK at *ca*. 80 °C and wafers washed in IPA for a couple of minutes, blow-dried and baked on a hotplate at *ca*. 130 °C for 10 min. Final cello-tape peel was performed to expose the fresh flake surface. For the polymer-treated flakes the following procedure was applied: a few millilitres of the PMMA solution were spin-coated onto the wafers at 3000 rpm for 60 s and baked on a hotplate at *ca*. 125 °C for 3 min. The polymerized PMMA was then removed by successive washes in acetone and IPA (10 min both) and wafer blow-dried. For the flakes transferred onto another substrate the following transfer procedure was applied: following the PMMA spin-coating, a cello-tape window was attached on top of the polymer to support it and a thin layer of underlying SiO_2 was dissolved using a dilute solution of KOH. The detached tape/PMMA/flake stack was then transferred onto the target substrate using a micromanipulator stage and optical microscope. A simplified schematic of the three different modes of preparation is depicted in figure 1.

Flake characterization
Graphene flakes were identified using an optical microscope and characterized with Raman spectroscopy using a Renishaw RM 264N94 spectrometer with 532 nm (2.33 eV) green YAG laser at $\leqslant$1 mW power and a Leica microscope with 100× objective, to distinguish between mono-, bi- and tri-layer graphene, and provide valuable information about strain and presence of lattice defects [22, 23]. Atomic force microscopy (AFM) was performed using a Multimode® 8, with an SNL-10 Si-tip on a Si_3N_4 cantilever. AFM imaging was performed in Peak Force tapping mode and Nanoscope Analysis software (v. 1.40) was used for analysis (all Bruker UK).

Results and discussion

Macroscopic and microscopic liquid-induced breakage of graphene
Liquid-induced flake damage was first noticed within our research group on graphene flakes prepared via 'standard' method, i.e. mechanical exfoliation of graphite onto oxygen plasma-cleaned silicon dioxide substrates. Large monolayer flakes, more than 100 μm

Figure 1. Schematic of three routes of monolayer graphene flake preparation: 'standard procedure' of exfoliating graphite onto oxygen plasma-treated SiO$_2$ substrate; 'PMMA treatment' consisting of spin-coating PMMA solution, polymerizing it at *ca.* 125 °C and subsequently dissolving it with acetone; and finally 'flake transfer' onto a target SiO$_2$ substrate, which had not been cleaned with oxygen plasma.

in lateral dimensions, were susceptible to breakage when covered in 0.1 M KCl aqueous solution [3]. Furthermore, this behaviour was later observed on a micrometre scale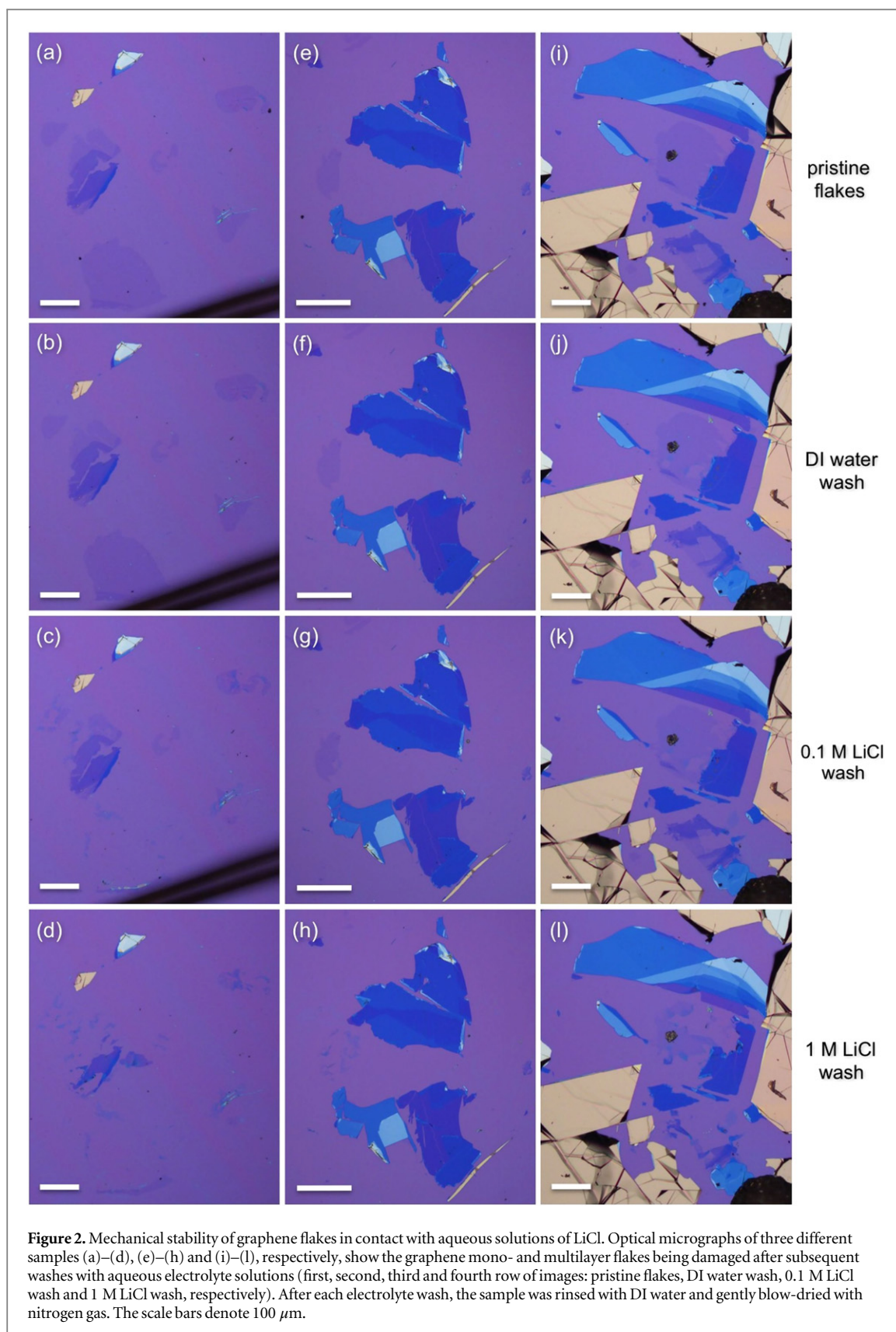 when individual liquid droplets deposited on the basal plane surface of monolayer graphene also induced flake damage [4, 5]. The damage was noted to occur in a variety of aqueous solutions, i.e. 1 M KCl, 6 M LiCl and 0.02 M tetra-ethylammonium chloride, and also organic solvents including glycerol, ethylene glycol and silicone oil [4]. We now extend these early observations to a detailed stability study of graphene upon exposure to aqueous electrolyte solutions. Figure 2 shows a series of optical micrographs demonstrating the damage, which occurs in mono- and multilayer graphene flakes after the entire sample was subsequently immersed in DI water, 0.1 M LiCl (aq.) and 1 M LiCl (aq.). The monolayer graphene flakes are visible in figure 2 as shadowy low-contrast patches, while thicker flakes have richer colours (violet, deep blue and turquoise correspond roughly to 2–10, 10–20 and 20–50 layers, respectively). It is evident that monolayer graphene (images of the pristine flakes in figures 2(a), (e) and (i)) incurred no or only minor damage when washed with DI water (figures 2(b), (f) and (j)). However, even a relatively low concentration of electrolyte solution is responsible for rupture of monolayer graphene and even thicker

flakes, which is more severe with increasing electrolyte concentration (figures 2(c)–(d), (g)–(h) and (k)–(l)).

In order to gain detailed understanding of the observed graphene breakage, a micromanipulator setup, allowing deposition of non-evaporating droplets of 6 M LiCl aqueous solution, was employed. Firstly, we find that the liquid-induced damage only affects monolayer graphene and does not occur on bilayer and thicker flakes. Figure 3 shows a flake, which is comprised of several areas consisting on mono, bi-, and tri/tetra-layers. Three stable droplets, measuring *ca.* 20 μm in diameter, were successfully deposited onto a bilayer graphene surface as shown in figure 3(a).

However, upon deposition on an adjacent mono-layer (green disk in figure 3(b)), the droplet spontaneously collapsed, and the liquid spread across the surface and induced permanent breakage of the graphene monolayer and surrounding multilayer areas. One of the droplets previously deposited on the bilayer maintained its original shape despite the extensive damage, suggesting the liquid forced its way under the bottom side of the flake. Figure 3(c) shows a detailed image of the damaged area and sites (coloured crosses) where supporting Raman spectra were recorded (figure 3(d)), identifying the number of graphene layers at each point through the use of the full width at

Figure 2. Mechanical stability of graphene flakes in contact with aqueous solutions of LiCl. Optical micrographs of three different samples (a)–(d), (e)–(h) and (i)–(l), respectively, show the graphene mono- and multilayer flakes being damaged after subsequent washes with aqueous electrolyte solutions (first, second, third and fourth row of images: pristine flakes, DI water wash, 0.1 M LiCl wash and 1 M LiCl wash, respectively). After each electrolyte wash, the sample was rinsed with DI water and gently blow-dried with nitrogen gas. The scale bars denote 100 μm.

half maximum (FWHM), shape, intensity, and frequency of the 2D band [24, 25]. Consistent observations on many individual flakes confirm that monolayer graphene is subject to significant breakage upon liquid deposition, which then often extends onto adjacent multi-layer areas. Graphene bilayer and thicker flakes are, however, resistant to damage upon contact with liquid, a phenomenon we would otherwise be unable to establish from macroscopic contact with liquid.
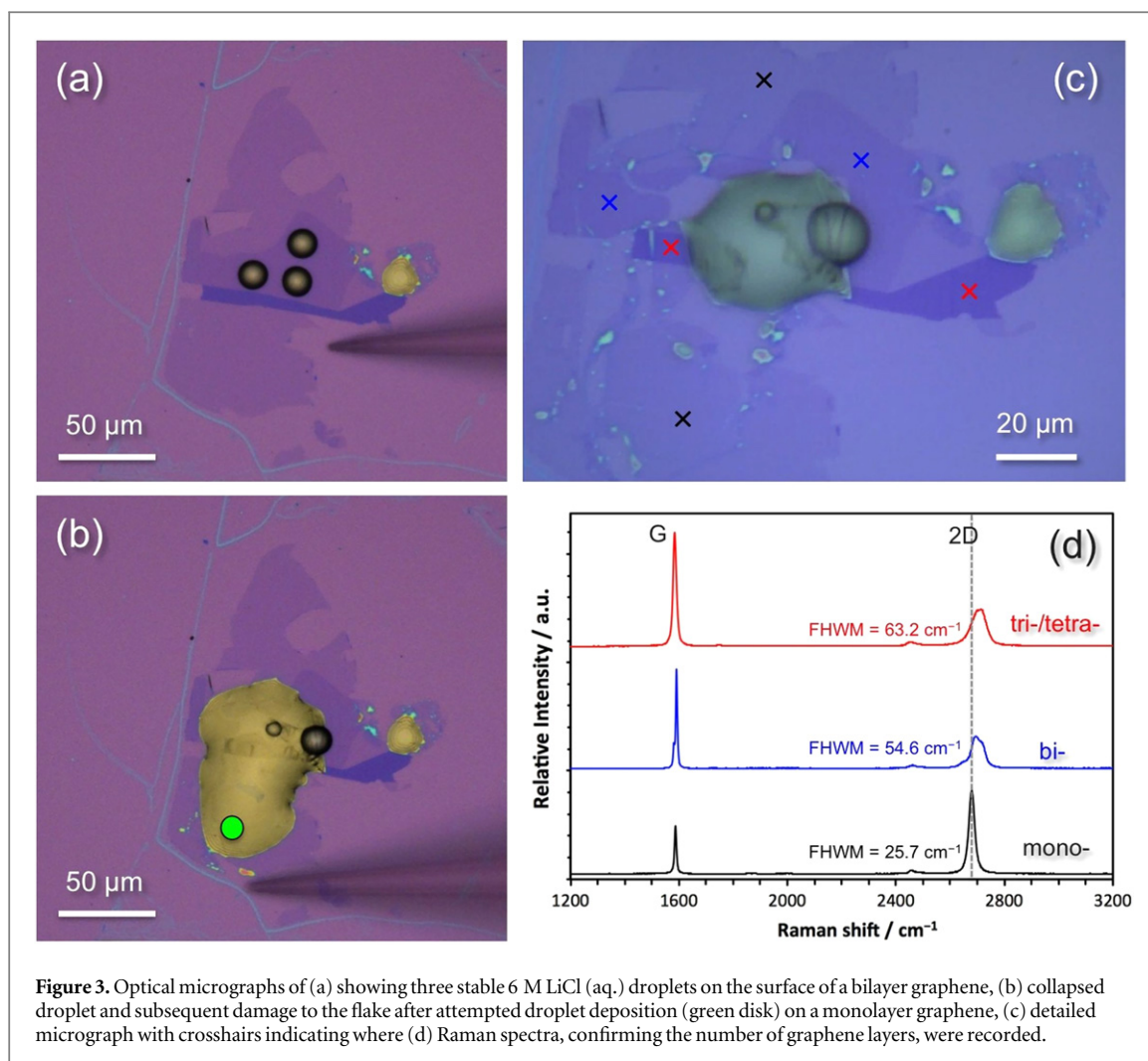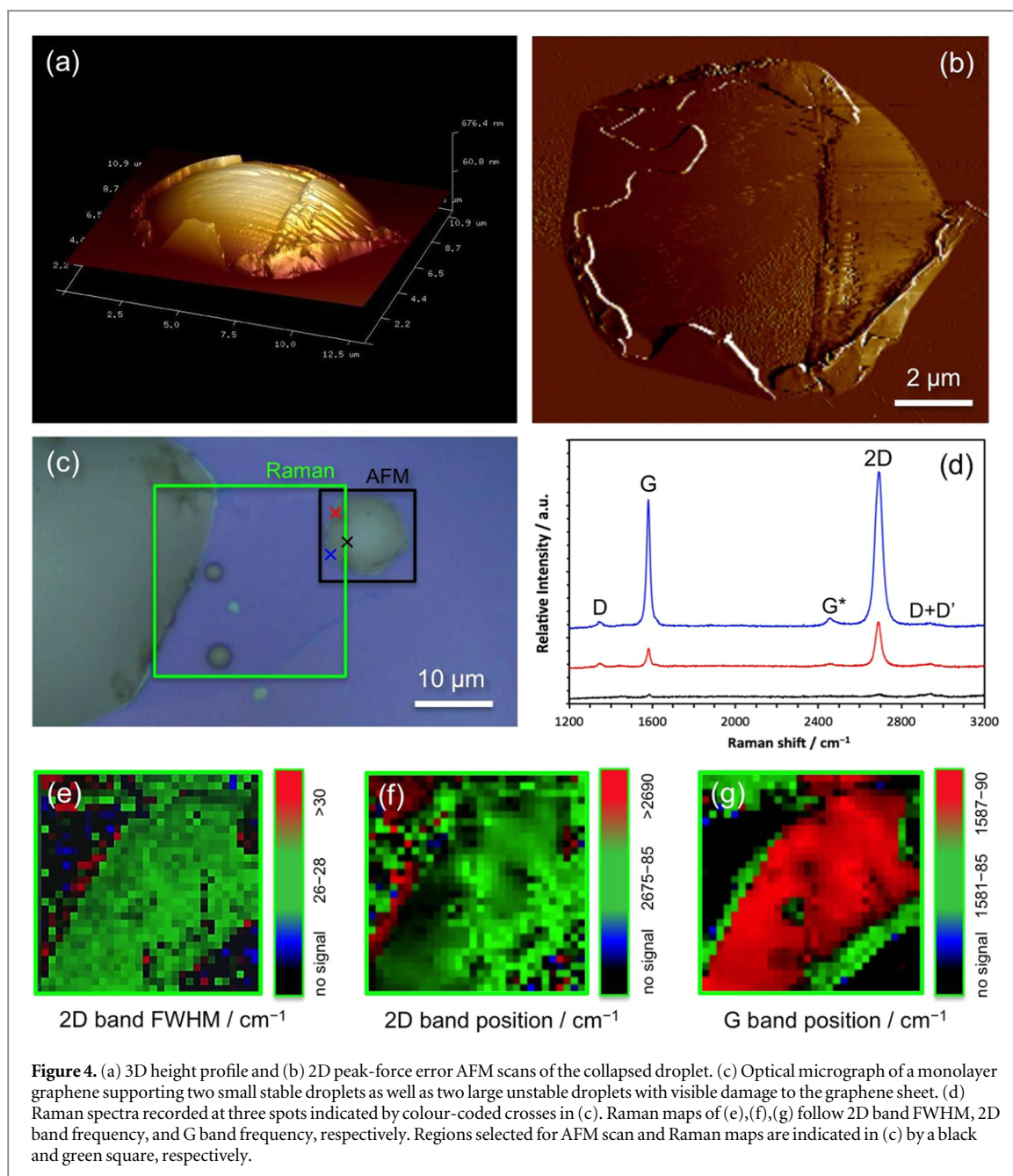
Figure 3. Optical micrographs of (a) showing three stable 6 M LiCl (aq.) droplets on the surface of a bilayer graphene, (b) collapsed droplet and subsequent damage to the flake after attempted droplet deposition (green disk) on a monolayer graphene, (c) detailed micrograph with crosshairs indicating where (d) Raman spectra, confirming the number of graphene layers, were recorded.

We suggest that the main parameter controlling droplet stability is the degree of strain imposed on the graphene sheet during droplet deposition, and subsequently, ways of dissipation of this strain in the crystal lattice of graphene. Oxygen plasma cleaning of the SiO_2 substrate, which is necessary for exfoliation of large flakes, yields a pristine hydrophilic surface, free of adventitious carbon, and exposes surface oxygen groups, which graphene can form bonds with. These bonds and strong adhesion forces between the plasma-cleaned substrate and graphene further reduce flexibility of the graphene sheet by pinning it in place, reduced its ability to compensate for external strain and making it prone to rupture. The key factors affecting the flake stability are: concentration of lattice defects in the graphene beneath the droplet, the area of the graphene–liquid interface, surface contamination, and the flexibility of the underlying graphene sheet. Indeed, it was found that smaller droplets were often more stable than larger ones, which is attributed to the smaller number of defects underlying the droplet; larger droplets, on the other hand, cover larger region of graphene and 'see' more defects contributing to droplet instability by permitting the liquid in contact with the underlying substrate and initiating the rupture. Furthermore, the damage occurred more often when the droplet encompassed the edge of graphene on the flake/substrate boundary, which is consistent with the large difference in contact angles between 6 M LiCl (aq.)/graphene (*ca.* 45–90°, graphene type and age dependent), and 6 M LiCl (aq.)/SiO_2 (*ca.* 20°) [4, 16]. The aqueous electrolyte solution favours more hydrophilic SiO_2, forces its way under the flake, either through the edge of graphene or lattice defect and triggers the observed damage. The number of layers significantly affects the stability of the droplets, as shown above. This can be attributed to shielding from the silica substrate provided by the top graphene layers; these additional layers minimize the numbers of defects exposing the liquid to the underlying silica substrate. Furthermore, the dissipation of strain originating from the liquid deposition is likely to be more efficient for multilayer flakes—graphene sheets can 'slide' and 'ripple' in respect to one another. This is supported by the fact that stress transfer between a substrate and a flake is much more efficient for monolayer graphene than graphite, as inferred from Raman spectroscopy of strained samples [26].

Figure 4. (a) 3D height profile and (b) 2D peak-force error AFM scans of the collapsed droplet. (c) Optical micrograph of a monolayer graphene supporting two small stable droplets as well as two large unstable droplets with visible damage to the graphene sheet. (d) Raman spectra recorded at three spots indicated by colour-coded crosses in (c). Raman maps of (e),(f),(g) follow 2D band FWHM, 2D band frequency, and G band frequency, respectively. Regions selected for AFM scan and Raman maps are indicated in (c) by a black and green square, respectively.

AFM and Raman spectroscopy of the ruptured graphene monolayer

The optical micrograph and AFM images in figure 4 reveal that the graphene monolayer underlying the collapsed droplets had become ruptured and torn, in contrast to the surface under the stable droplets where graphene remained intact. This results in excessive wetting and subsequent reduction in droplet height, which permits AFM measurement of the damaged flake (figures 4(a) and (b)). The induced damage is significant, with the middle region of the underlying graphene completely torn apart. Raman spectroscopic mapping was employed to assess the extent of liquid-induced strain in the graphene sheet (green square in figure 4(c) indicates the selected area). The Raman map in figure 4(e) follows the width of the 2D band, with the green colour corresponding to a

FWHM = 26–28 cm^{-1}, which matches that of mono-layer graphene [24, 25]. Red corresponds to 2D peak broadening to FWHM greater than 30 cm^{-1}, indicating generic strain in the graphene flake [27], and, finally, black/blue colours represent regions in which no 2D band signal was observed. Indeed, the green colour in figure 4(e) corresponds to undamaged graphene, visible in the optical micrograph, and the areas at the edges of the collapsed liquid droplets experience a measureable degree of lattice strain (red). The interiors of both the collapsed droplets show little or no Raman signal (blue/black), confirming that the graphene sheet curls and folds itself at the edge of the drop. The strain experienced by the graphene sheet is also expressed by the Raman map in figure 4(f), which follows the 2D band frequency. Here, green corresponds to frequencies of 2675–2685 cm^{-1} (pristine

monolayer), whereas red indicates values greater than 2690 cm^{-1} (strained monolayer), and, as previously, black/blue represent no measured signal. Importantly, the blueshift in the 2D band frequency suggests that the graphene sheet experiences compressive strain, which is expected from the visible graphene folding and buckling. This was shown by purposely controlling both uniaxial [26, 28, 29] and biaxial [30] strain in graphene. Furthermore, figure 4(g) shows a Raman map of a G band frequency, where black indicates no signal, red corresponds to 1587–1590 cm^{-1}, and green/blue corresponds to 1581–1585 cm^{-1}, indicating redshift in the strained parts of the flake.

The Raman analysis shows that the 2D band frequency increases with strain whereas the G band shows the opposite trend, i.e. decrease in frequency. While the same blueshift trend is observed for both 2D and G bands in the case of compressive strain in monocrystalline ME graphene [29, 30], an opposite trend, i.e. blueshift (2D) and redshift (G) is observed for CVD graphene, which is explained by the polycrystallinity of such samples [27, 31]. The latter observation is consistent with our results as the damaged parts of graphene in figure 4 are clearly torn apart into many small folded flakes. Note that the G band FWHM also increases with the decrease its frequency, ruling out any significant doping, which would have the opposite effect [32]. Finally, the D and D + D′ bands appear in the full Raman spectra of figure 4(d), recorded on the edges of the collapsed droplet (red and blue crosses in figure 4(c)), indicating presence of lattice defects [22, 23].

The effect of transfer procedure and polymer residues on graphene stability

It was also discovered that transfer of graphene flakes onto another SiO$_2$ substrate increased resistance of monolayer graphene towards liquid-induced damage. A PMMA polymer was used as an aid to transfer the flakes to another SiO$_2$ substrate, which was not previously treated with oxygen plasma. The transfer process enabled deposition of stable droplets on the basal plane of graphene with success rates over 75%, as shown in figure 5(a) (droplets marked with green arrows). The stable droplets maintain a spherical shape with no obvious changes to the graphene flake underneath. Unstable droplets either trigger extensive damage to graphene as in the case in figures 3(b) and (c) or results in a collapse of a droplet and visible rupture of underlying graphene (droplets marked with red arrows). In addition, some of the stable droplets make visible ripples in the graphene sheet appear, as seen in figure 5(a) (marked with yellow arrows). These ripples were never observed on graphene prepared the 'standard' way and it is likely that they would collapse immediately due to inability of 'standard' graphene flakes to dissipate the strain. It is worth noting that no liquid-induced damage was observed to graphene monolayer transferred to other atomically-flat target

substrates including h-BN and MoS$_2$. It is clear that the treatment of flakes with PMMA, and subsequent transfer onto a substrate untreated with oxygen plasma, does significantly improve their stability.

Flakes transferred from the original, plasma-treated SiO$_2$ substrate to a plasma-untreated SiO$_2$ substrate have two main differences from the flakes prepared using the 'standard' method: (A) PMMA polymer residues leftover from the transfer process are notoriously difficult to remove and some remain on the flake surface [15, 33–36], and (B) since the plasma cleaning stage of SiO$_2$ substrate is omitted, some contaminants leftover after the imperfect solvent cleaning of the SiO$_2$ wafer are trapped between graphene and the underlying substrate. The difference between these two cleaning methods is supported by the AFM images in figure 6: the plasma cleaning results in much smoother surface than the sole solvent washing. The AFM image in figure 5(b) shows the surface of a monolayer graphene flake after transfer using a PMMA mask: the surface-bound residues are clearly visible. In order to examine the effects of PMMA debris on graphene-droplet stability alone, a monolayer flake prepared using the 'standard' way was spin-coated with PMMA, which was subsequently dissolved with acetone and IPA. It can be seen in figure 5(c) that although some of the deposited droplets remain stable, more than 70% of droplets had collapsed with associated damage to PMMA-treated graphene, in comparison to only *ca.* 25% failure rate of the same experiment on the 'transferred' flakes as shown in figure 5(a).

In summary, it was found that graphene prepared via the 'standard' method rarely permits stable deposition of aqueous electrolyte solution on its basal plane without causing underlying flake damage, yet PMMA residues enhance the mechanical stability of graphene. Furthermore, transfer onto chemically identical substrates, but untreated with oxygen plasma, has an even more pronounced effect. Interestingly, formation of polar surface groups on plasma-cleaned SiO$_2$ substrate (compared to as-received SiO$_2$), leads to increase in overlaying graphene reactivity, attributed to formation of electron–hole puddles [37]. The above observations suggest that the mechanism of monolayer stabilization is, in principle, related to the surface contamination of the sample. This contamination, both on top of the flake and trapped between the flake and substrate allows the strain to be dissipated more easily and in essence makes the graphene sheet less brittle and more flexible. It has been shown that flakes in contact with PMMA from one, or even more so, from both sides, can withstand significant tensile and compressive strain, up to *ca.* 1%, which prevents graphene from collapsing and buckling [26]. Furthermore, friction between SiO$_2$ substrate and graphene monolayer/bilayer has been shown to be inversely proportional to strain [38], which explains how PMMA residues, which introduce small level of pre-strain upon curing of the polymer, allow graphene to slide more easily on
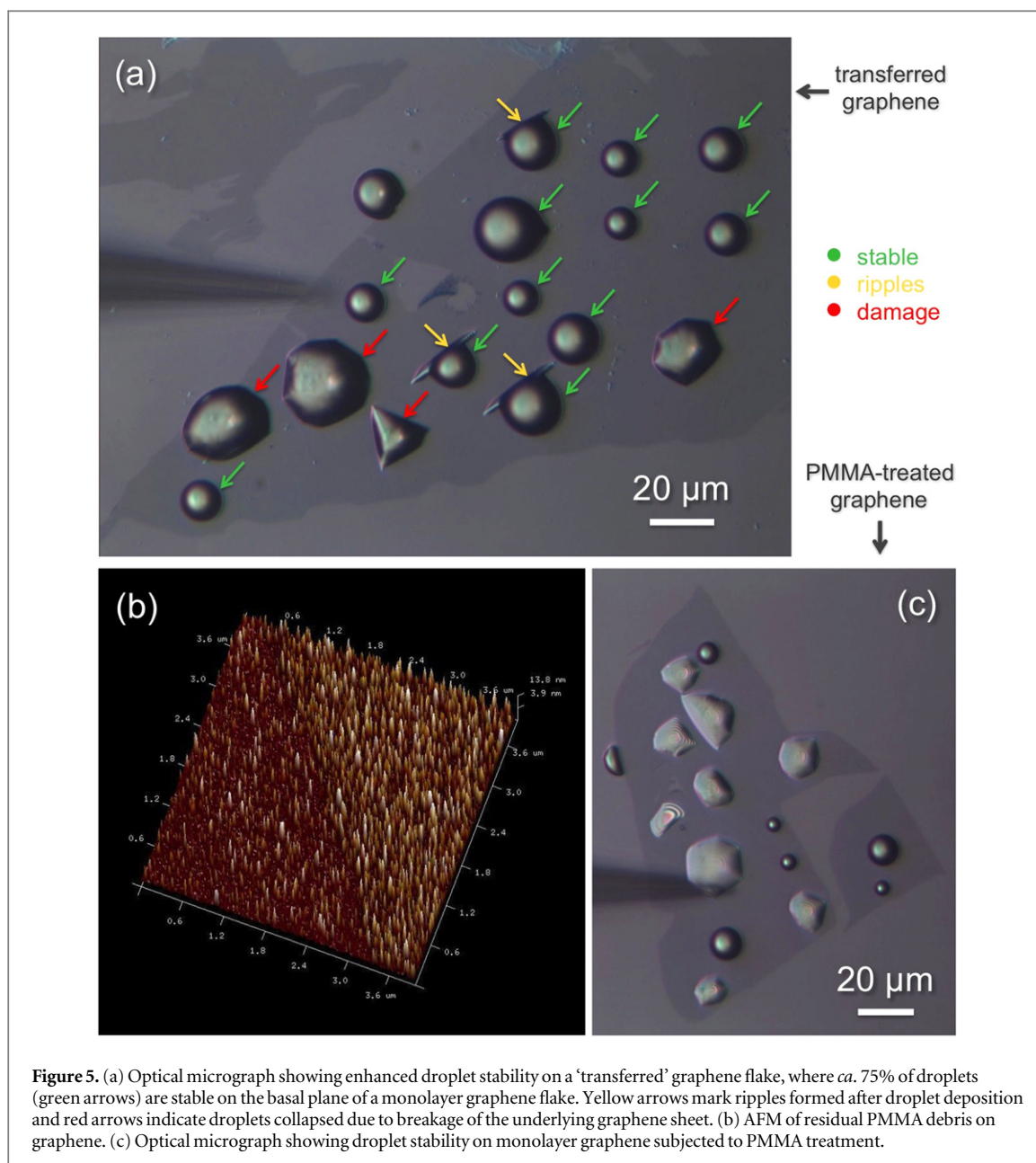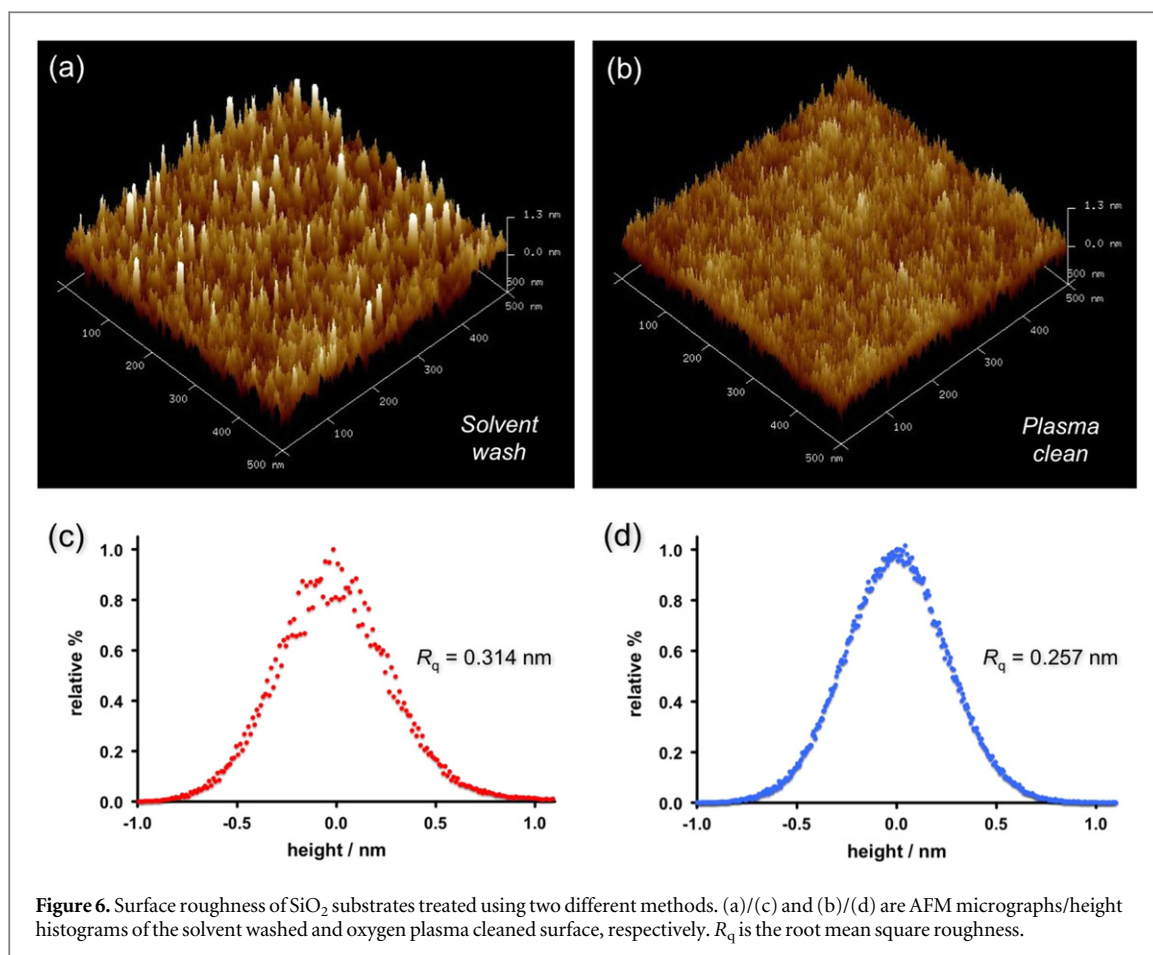
Figure 5. (a) Optical micrograph showing enhanced droplet stability on a 'transferred' graphene flake, where *ca.* 75% of droplets (green arrows) are stable on the basal plane of a monolayer graphene flake. Yellow arrows mark ripples formed after droplet deposition and red arrows indicate droplets collapsed due to breakage of the underlying graphene sheet. (b) AFM of residual PMMA debris on graphene. (c) Optical micrograph showing droplet stability on monolayer graphene subjected to PMMA treatment.

the substrate and dissipate the stress from liquid deposition efficiently. This is supported by no signs of liquid-induced damage of graphene exfoliated directly on PMMA substrate, also previously confirmed for graphene transferred to SU8 photoresist [4]. It is also worth noting that no liquid-induced damage was observed for monolayer CVD graphene [11, 12]. This can be explained, according to our rationalization above, by the inherent polycrystallinity of CVD graphene and presence of PMMA residue from the transfer process, both of which contribute to more effective dissipation of lattice strain.

Conclusions

In this paper we aim to draw attention to the irreversible damage caused to the SiO_2-bound graphene monolayer upon contact with aqueous electrolyte solutions. It was found that while immersing the samples in DI water rarely changed the flake, relatively low concentration of aqueous electrolyte triggered breakage of the mono- and multilayer graphene flakes. Employing a localized microdroplet deposition using 6 M LiCl aqueous solution revealed that the liquid droplets were stable when deposited on flakes ranging from graphite to bilayer graphene, but collapsed and caused significant flake damage to monolayer graphene. The damage could be supressed via polymer debris or through transfer of flakes on another SiO_2 substrate that has not been subjected to oxygen plasma cleaning. It is suspected that the liquid-induced damage is defect driven, and there are several factors which therefore influence droplet stability on these systems; the mechanical stiffness of the additional graphene layers can considerably stabilise

Figure 6. Surface roughness of SiO$_2$ substrates treated using two different methods. (a)/(c) and (b)/(d) are AFM micrographs/height histograms of the solvent washed and oxygen plasma cleaned surface, respectively. R_q is the root mean square roughness.

droplets by minimizing the effect of lattice defects, which act as gateways toward splitting of graphene from the underlying silica substrate. The polymer residues and impurities introduced during the flake transfer have stabilizing effect on droplet formation, permitting contact between graphene and a liquid, for example in electrochemistry or corrosion protection.

Acknowledgments

References

[1] Novoselov K S, Fal'ko V I, Colombo L, Gellert P R, Schwab M G and Kim K 2012 *Nature* **490** 192–200

[2] Li W, Tan C, Lowe M A, Abruña H D and Ralph D C 2011 *ACS Nano* **5** 2264–70

[3] Valota A T, Kinloch I A, Novoselov K S, Casiraghi C, Eckmann A, Hill E W and Dryfe R A W 2011 *ACS Nano* **5** 8809–15

[4] Toth P S, Valota A, Velický M, Kinloch I, Novoselov K, Hill E W and Dryfe R A W 2014 *Chem. Sci.* **5** 582–9

[5] Velický M *et al* 2014 *ACS Nano* **8** 10089–100

[6] Wang J, Yang S, Guo D, Yu P, Li D, Ye J and Mao L 2009 *Electrochem. Commun.* **11** 1892–5

[7] Ambrosi A, Bonanni A and Pumera M 2011 *Nanoscale* **3** 2256–60

[8] Brownson D A C, Munro L J, Kampouris D K and Banks C E 2011 *RSC Adv.* **1** 978–88

[9] Zhang B, Fan L, Zhong H, Liu Y and Chen S 2013 *J. Am. Chem. Soc.* **135** 10073–80

[10] Güell A G, Ebejer N, Snowden M E, MacPherson J V and Unwin P R 2012 *J. Am. Chem. Soc.* **134** 7258–61

[11] Tan C, Rodríguez-López J, Parks J J, Ritzert N L, Ralph D C and Abruña H D 2012 *ACS Nano* **6** 3070–9

[12] Valota A T, Toth P S, Kim Y J, Hong B H, Kinloch I A, Novoselov K S, Hill E W and Dryfe R A W 2013 *Electrochim. Acta* **110** 9–15

[13] Feng X, Maier S and Salmeron M 2012 *J. Am. Chem. Soc.* **134** 5662–8

[14] Barr T L and Seal S 1995 *J. Vac. Sci. Technol.* A **13** 1239–46

[15] Patten H V, Velicky M, Clark N, Muryn C A, Kinloch I A and Dryfe R A W 2014 *Faraday Discuss.* **172** 261–71

[16] Li Z *et al* 2013 *Nat. Mater.* **12** 925–31

[17] Rafiee J, Mi X, Gullapalli H, Thomas A V, Yavari F, Shi Y, Ajayan P M and Koratkar N A 2012 *Nat. Mater.* **11** 217–22

[18] Shih C J, Wang Q H, Lin S, Park K C, Jin Z, Strano M S and Blankschtein D 2012 *Phys. Rev. Lett.* **109** 176101

[19] Chang C H, Huang T C, Peng C W, Yeh T C, Lu H I, Hung W I, Weng C J, Yang T I and Yeh J M 2012 *Carbon* **50** 5044–51

[20] Schriver M, Regan W, Gannett W J, Zaniewski A M, Crommie M F and Zettl A 2013 *ACS Nano* **7** 5763–8

[21] Singh Raman R K, Chakraborty Banerjee P, Lobo D E, Gullapalli H, Sumandasa M, Kumar A, Choudhary L, Tkacz R, Ajayan P M and Majumder M 2012 *Carbon* **50** 4040–5

[22] Ferrari A C 2007 *Solid State Commun.* **143** 47–57

[23] Malard L M, Pimenta M A, Dresselhaus G and Dresselhaus M S 2009 *Phys. Rep.* **473** 51–87

[24] Ferrari A C *et al* 2006 *Phys. Rev. Lett.* **97** 187401

[25] Park J S, Reina A, Saito R, Kong J, Dresselhaus G and Dresselhaus M S 2009 *Carbon* **47** 1303–10

[26] Tsoukleri G, Parthenios J, Papagelis K, Jalil R, Ferrari A C, Geim A K, Novoselov K S and Galiotis C 2009 *Small* **5** 2397–402

[27] Bissett M A, Tsuji M and Ago H 2013 *J. Phys. Chem.* C **117** 3152–9

[28] Bissett M A, Tsuji M and Ago H 2014 *Phys. Chem. Chem. Phys.* **16** 11124–38

[29] Frank O, Tsoukleri G, Parthenios J, Papagelis K, Riaz I, Jalil R, Novoselov K S and Galiotis C 2010 *ACS Nano* **4** 3131–8

[30] Ding F, Ji H, Chen Y, Herklotz A, Dörr K, Mei Y, Rastelli A and Schmidt O G 2010 *Nano Lett.* **10** 3453–8

[31] Bissett M A, Izumida W, Saito R and Ago H 2012 *ACS Nano* **6** 10229–38

[32] Das A *et al* 2008 *Nat. Nanotechnology* **3** 210–5

[33] Her M, Beams R and Novotny L 2013 *Phys. Lett. A: Gen. At. Solid State Phys.* **377** 1455–8

[34] Pirkle A, Chan J, Venugopal A, Hinojos D, Magnuson C W, McDonnell S, Colombo L, Vogel E M, Ruoff R S and Wallace R M 2011 *Appl. Phys. Lett.* **99** 122108

[35] Suk J W, Lee W H, Lee J, Chou H, Piner R D, Hao Y, Akinwande D and Ruoff R S 2013 *Nano Lett.* **13** 1462–7

[36] Lin Y C, Lu C C, Yeh C H, Jin C, Suenaga K and Chiu P W 2012 *Nano Lett.* **12** 414–9

[37] Wang Q H *et al* 2012 *Nat. Chem.* **4** 724–32

[38] Kitt A L, Qi Z, Rémi S, Park H S, Swan A K and Goldberg B B 2013 *Nano Lett.* **13** 2605–10